International Journal of Soft Computing and Engineering (IJSCE)
ISSN: 2231-2307, Volume-2, Issue-1, March 2012

Fast and Slow Transient Response of WECS with Simultaneous Actions

M.Amarendra, S.Srikanth, G. Siva Suteja, B.Prasanna lakshmi, K.Madhavi latha

Abstract— This paper details the transient operation of a wind energy conversion system (WECS) used simultaneously as an ac- tive filter and power generator. This study is intended to address the system response to two types of transient phenomena: voltage dips (fast transients) and wind speed variations (slow transients). The system response to voltage dips is governed by the electrical system dynamics and control method and results in the evaluation of the WECS low-voltage ride through capability. The study of the system response to wind speed variations requires a complete mechanical model to be included. Simulation results are presented for a typical WECS, and a discussion is carried out dealing with the generalization of the present work to other configurations.

***Index Terms*—Doubly fed induction generator(DFIG), Harmonic compensation, Low- voltage ride through (LVRT), Transients, Wind energy conversion systems(WECSs).**

I. BACKGROUND

WIND energy conversion systems (WECSs) are an es tablished power generation technology that is evolving from being just an alternative energy source to providing morevcomplex functions, such as reactive power supply, voltage con- trol, and active power regulation [1]. These additional functions (known as ancillary services) are possible due to the improve- ment of solid-state devices performance and the advancement in control system design [2].

One of the ancillary services is the use of WECS as an ac- tive filter (AF) [3], [4]: the power converters installed in the WECS are controlled to sink the harmonic currents injected by nonlinear loads (NLLs) connected at the same point of com- mon coupling (PCC); at the same time, the WECS delivers fundamental active power extracted from the wind. The steady- state performance of WECS used simultaneously as an AF, and power generator has been analyzed in [5]–[9]. The present pa- per is intended to investigate the transient response of a WECS performing AF analyzed in [5]–[9]. The present pa- per is intended to investigate the transient response of a WECS performing AF operation, following voltage dips or wind speed variations.

The studied system is shown in Fig. 1. The doubly fed induction generator (DFIG) stator terminals are connected to the PCC through a feeder, represented by the equivalent resistance R_c and inductance L_c. The DFIG rotor is supplied by two back- to-back connected converters: the rotor side converter (RSC) and the line side converter (LSC). The feeder that connects the

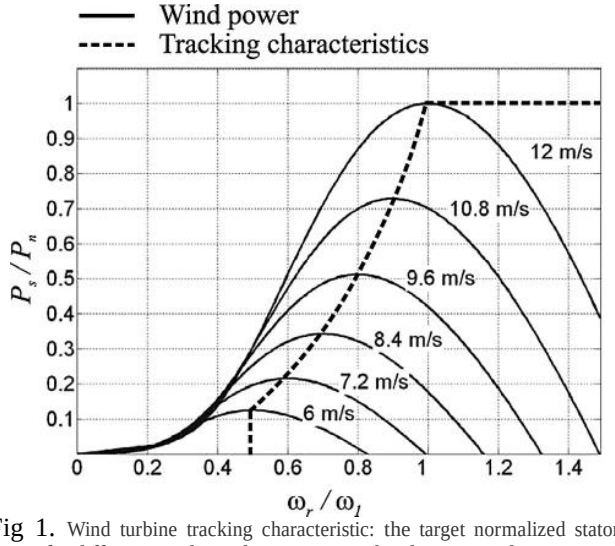

Fig 1. Wind turbine tracking characteristic: the target normalized stator power for different wind speeds versus normalized rotor speed.

TABLE I
SYSTEM
PARAMETERS

DFIG	P_n = 1.50 MW, $cos\varphi_n$ = 0.90, V_n = 575 V , number of poles = 6, R_s = 0.00706 p.u., L_{ls} = 0.171 p.u., R_r = 0.005 p.u., L_{lr} = 0.156 p.u., L_m = 2.9 p.u., H (inertia constant) = 5.04 s, F (friction factor) = 0.01 p.u.
Supply line	V_n = 600 V, f_n = 60 Hz, R_g = 0.1153 Ω/km, L_g = 1.05 mH/Km
RSC,LSC and dc-link	C = 0.6 F, V_{dc} = 1200 V, R_L = 3 mΩ, L_L = 300 mH, f_{sw} =6480 Hz. IGBTs characteristics as in [11].
Two mass model	Generator inertia J_r = 5.04 s, turbine inertia J_t = 4.45 s, torsional spring constant k = 0.001 N/m.

M.Amarendra, Associate professor, Department ofEEE, KITS, Guntur, A.P., India.
S.Srikanth, Assistant Professor, Sri Vani School of Engineering, Vijayawada, A.P., India.
G. Siva suteja (M.Tech), Department of EEE, MIC College of Technology, Vijayawada, A.P., India.
B.Prasanna lakshmi (M.Tech), Department of EEE, MIC College of Technology, Vijayawada,A.P.,India.
K.Madhavi latha(M.Tech), Department of EEE,Sasi Institute of Engineering & Ttechnology,West Godavari,A.P.,India.

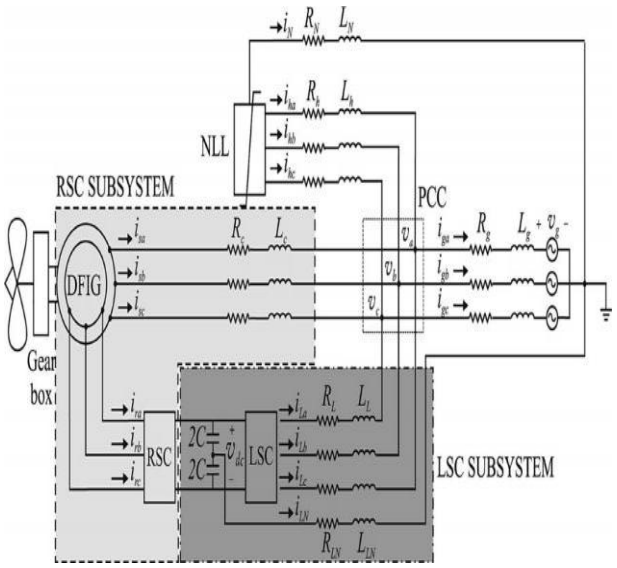

Fig.:-2

LSC to the PCC has the equivalent resistance R_L and inductance L_L. The RSC and LSC solid-state switches are driven by means of pulse width modulation (PWM) [10]. The dc-link is made of two series-connected capacitors, and the centered tap is connected to the neutral.

A NLL is connected to the same PCC through a feeder, rep- resented by the equivalent resistance R_h and inductance L_h. On the right side of the three-phase diagram presented in Fig. 1, the step-up transformer and supply line Thevenin equivalent circuit is shown.

The system parameters are listed in Table I; the tracking characteristic is shown in Fig. 2.

II. COMPENSATION BY MEANS OF COMBINED MODULATION

The WECSs based on DFIG include two power converters, and this design allows different approaches to AF implementation: in [8], three different control systems are described in detail and compared. It has been concluded that the most effec- tive AF strategy uses both power converters and the DFIG to sink harmonic currents injected by the NLL; this strategy is named "compensation by means of combined modulation (CM)."

The control system is designed in an equivalent $dq0$ domain [4], [12]: NLL harmonic currents and power extracted from the wind are the input for the block diagrams that control the RSC and LSC; these block diagrams presented and described in [13] and [8]. When compensation by means of CM is applied, cancellation of the positive- and negative-sequence harmonics is obtained by means of RSC modulation, and cancellation of zero-sequence harmonics is obtained by means of LSC modulation.

Steady-state analysis shows that the proposed application has two main effects on WECS operation:

1) Power loss increase: harmonic current flow results in ad- ditional winding and solid-state switches loss;
2) Voltage distortion: harmonic current flow causes harmonic voltage drop on the line connecting the WECS to the PCC. This condition leads to peak voltages at the stator and power converter terminals exceeding the rated values.

The power loss increase requires WECS derating for wind speeds above the design value ($v_{w,n}$ =12 m/s for the turbine assumed in the present study, Fig. 2) [13]. Voltage distortion and consequent peak voltages that exceed the rated value require a conservative choice of WECS components, in particular of the solid-state devices.

III. SYSTEM OPERATION ASSESSMENT

The WECS operation at the instant when a disturbance (either voltage variation or wind speed variation) takes place is defined by the wind speed value and the NLL current spectrum. The following conditions are assumed in the present work

1) The NLL consists of three single-phase diode bridges con-
nected line-to-neutral: the dc-load current is 480 A. Since this load injects positive-, negative-, and zero-sequence harmonic currents, both the LSC and the RSC are mod- ulated to sink harmonic currents components. Table II presents the THD [14] improvement obtained by applying compensation by means of CM [8].
2) The wind speed is 18 m/s, corresponding to the maximum normalized rotor speed $\omega_r/\omega_1 = 1.5$ p.u. and con- sequent maximum fundamental power flow within the WECS components.
3) For the assumed NLL and normalized rotor speed, it is proved in [8] that derating D =0.85 is necessary.

The software used for simulations is MATLAB/Simulink; a fixed step solver is used, with time step $T = 50\ \mu$s.

Table II CURRENT AND VOLTAGE THD AT THE PCC FOR THE ASSUMED NLL, WITHOUT HARMONIC COMPENSATION AND WITH COMPENSATION BY MEANS OF CM

THD	No Comp.	CM	% Difference
Voltage	0.24	0.030	87.5%
Current	0.10	0.055	−45.0%

IV. SYSTEM RESPONSE TO VOLTAGE DIPS

The most recent international standards [15] require the WECSs to remain connected to the grid after a voltage sag takes place and to continue to supply power; this requirement is known as "low-voltage ride through" (LVRT). For the US, LVRT requirement is defined in the FERC order 661A "Standard pro- cedures and technical requirements for the interconnection of large wind generation" [16].

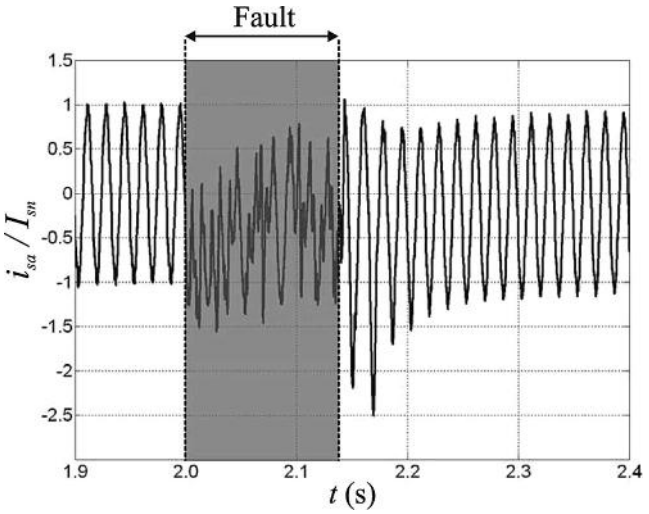

Fig. 3. Symmetrical fault: normalized stator current oscillogram, compensa- tion by means of CM is applied.

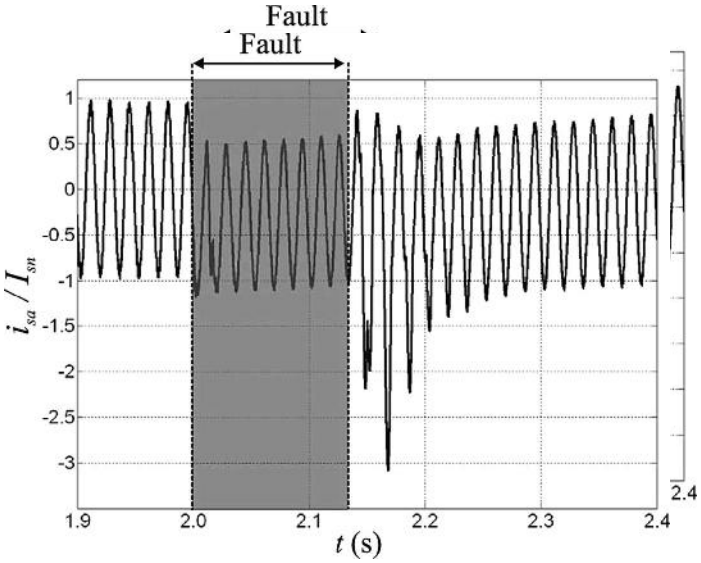

Fig. 4. Symmetrical fault: normalized stator current oscillogram, no harmonic compensation is applied.

Many studies have been carried out to assess the LVRT ability of WECSs based on DFIG technology [17]–[19]; the present analysis is intended to determine the effects of AF operation on the WECS response following voltage dips.

A. Simulation results—Oscillograms

According to [16], the most severe fault conditions are defined as follows: "The maximum clearing time the wind generating plant shall be required to withstand for a three-phase fault shall be 9 cycles ... A wind generating plant shall remain intercon- nected during such a fault on the transmission system for a voltage level as low as zero volts." The system response to the fault described earlier is presented in this section by means of oscillograms of the most significant quantities.

The stator current oscillogram is shown in Fig. 3, for the phase with the largest transient current amplitude. Two separate regions are identified.

1) $2 \leq t \leq 2.15$ s (transient during the fault).The current pattern is determined by DFIG demagnetization [20];
2) $t \geq 2.15$ s (transient following fault clearance). The peak current is obtained as the sum of two contributions: DFIG magnetization and phase shift restoration between the fun- damental voltage phasors at the PCC and at the stator terminals.

The normalized peak stator current is approximately 2.5 p.u., and it is measured after fault clearance. Since the transient dies out in a few cycles and the heating process is adiabatic, the power loss caused by this fault is not detrimental for winding insulation properties [13]. However, the large peak current causes magnetic forces that may damage the winding insulation.

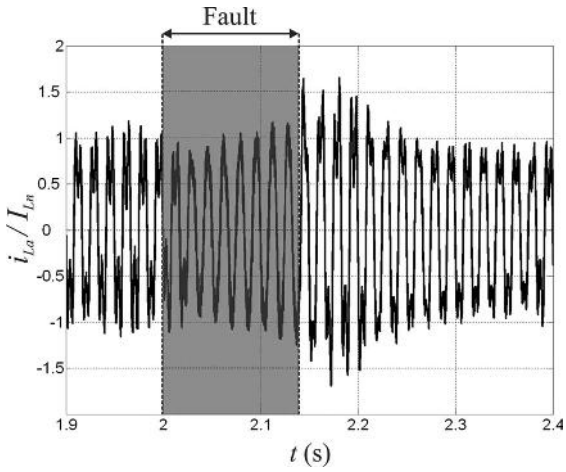

Fig. 5. Symmetrical fault: normalized LSC current oscillogram, compensation by means of CM is applied

To assess the effects of AF operation on WECS performance, the stator current is monitored for the same fault when the WECS is not providing harmonic compensation. Under this condition, the sinusoidal rated stator current is supplied by the generator, and derating is not applied. Normalized stator current obtained for sinusoidal operation is presented in Fig. 4. Similarly to Fig. 3, two regions can be identified; however, the current waveform is cleaner than the one shown in Fig. 3, since the stator is not injecting any harmonic currents. By comparing Figs. 3 and 4, one concludes that the peak current value is higher in the case of sinusoidal operation. This result is explained by observing that derating is applied when CM is implemented, thus causing a reduction of the fundamental current amplitude with respect to sinusoidal operation both in steady-state operation and during the transients.

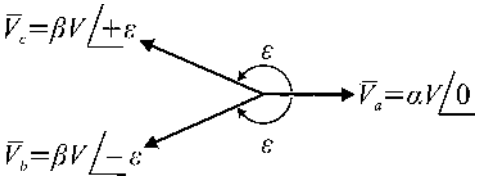

Fig. 6. Voltage phasor diagram used to describe seven fault types listed in [21]. α and β are the scale parameters, ε is the phase angle.

TABLE III
FAULT CHARACTERISTICS FOR THE PHASOR DIAGRAM SHOWN IN FIG. 6

Type	α	β	ε
Three-phase	0 to 1	α	120 deg
Single-phase	0 to 1	1	120 deg
Phase-to-phase	1	0 to 1	0 to 180 deg

In Fig. 5, LSC current oscillogram is illustrated. LSC current rises during the fault, since fundamental power flow through the stator is reduced and the fraction of power flowing through the rotor and the power converters increases. After the fault clear- ance, a second transient takes place to restore the prefault power distribution. The current increase through the power converters following a voltage dip is a critical variable, since the solid- state devices [insulated gate bipolar transistors (IGBTs) for the present study] are very sensitive to increasing power loss and temperature.

B. Simulation Results—Contour Plots

The overall system response to voltage dips is studied for a set of different fault conditions, described by three characteristics: topology (phase-to-ground, two-phase, three-phase, and phase shift), residual voltage amplitude (from 0 to 1 p.u.), and fault duration (from 0 to several seconds). Fig. 6 displays the three parameters used to characterize the fault:

1) ***Sag* amplitude** α,β. The parameters α and β determine the magnitude of phasors V_a, V_b, and V_c, correspond- ing to the line-to-neutral phase voltages at the high side of the step-up transformer. The values of α and β for different types of faults are listed in Table III. For three- phase symmetrical faults $\alpha = \beta$; for phase-to-ground sag $0 \leq \alpha \leq 1$ and $\beta = 1$ (only the magnitude of phase a volt- age changes). For phase-to-phase sags, $0 \leq \beta \leq 1$ and $\alpha = 1$ (the magnitude of phases b and c voltage changes with the same ratio). Asymmetrical faults are described by the simultaneous variation of α and β.

2) ***Phase angle*** ε. Phase angle ε is the angle measured be- tween phase a voltage and either phase b or c voltage. The value of ε during a fault is determined by the type of three-phase transformers installed between the fault lo- cation and the PCC. In practice, only a few degrees of variation around the rated value are observed [21].

3) ***Sag duration*** Δt. Sag duration may vary from 0 ms to 3s. This range of values is chosen according to the LVRT curve displayed in Fig. 7[1] according to a Wester Energy Coordinating Council (WECC) white paper [23].

A set of contour plots is used to present the system response to faults. This presentation has been chosen to give a complete overview of the system behavior.

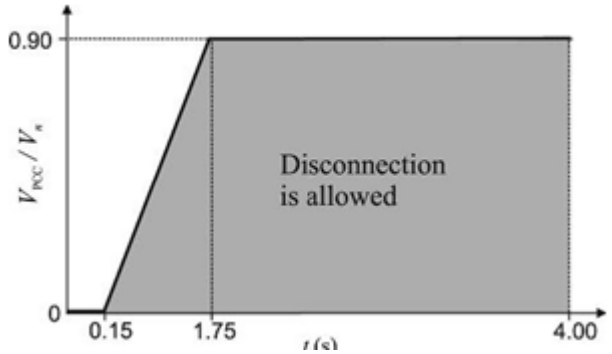

Fig. 7. LVRT curve according to the WECC white paper: the voltage at the PCC is plotted as function of time. Disconnection of the WECS is allowed in the gray region.

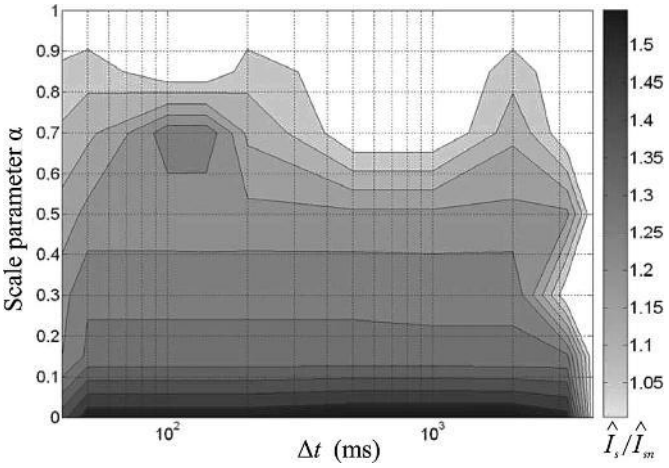

Fig. 8. Phase-to-ground sag: normalized stator current; *x*-axis: fault duration, *y*-axis: scale parameter α.

In Fig. 8, the contour plot illustrates the normalized peak stator current during phase-to-ground faults with varying am- plitude and duration. The *x*-axis uses a logarithmic timescale to present the fault duration Δt; the *y*-axis measures the nor- malized residual voltage amplitude α. The gray scale on the right shows the normalized stator peak current amplitude for the phase with maximum current. For $\alpha < 0.025$, the maximum value of normalized peak stator current for a phase-to-ground fault is approximately 1.55 p.u.

The normalized peak stator current contour plot for symmet- rical faults is displayed in Fig. 9. For $\Delta t = 150$ ms (nine cycles) and $\alpha = \beta = 0$, the stator peak current amplitude is approxi- mately 2.5 p.u., in agreement with Fig. 3. Fig. 9 shows that for relatively high residual voltage amplitudes (above 0.15 p.u.), the time of reclosure determines the peak stator current amplitude. In contrast, for small values of α and β, the fault duration Δt has more impact than the residual voltage in determining the peak current amplitude. This result can be justified by observing that a small residual voltage causes the air-gap rotating field within the machine to extinguish, thus causing severe transient currents in the stator windings.

While the analysis of the voltage oscillograms results in the conclusion that stator overcurrent dies out in a few cycles, the contour plot allows summarizing the peak current ampli- tude and evaluating magnetic forces between conductors for a large quantity of faults, thus giving information needed for mechanical design of the windings.

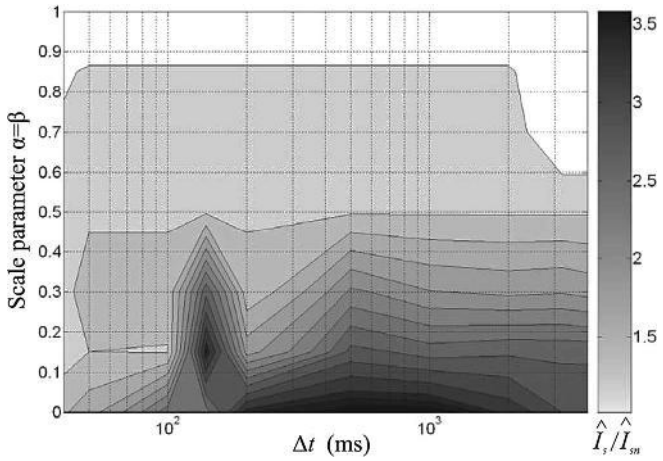

Fig. 9. Symmetrical sag: normalized stator current; x-axis: fault duration, y-axis: scale parameter $\alpha = \beta$

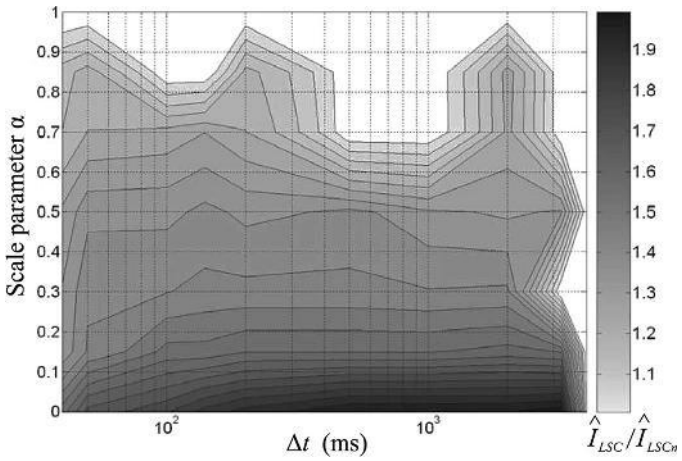

Fig. 10. Phase-to-ground sag: normalized LSC peak current contour plot. x-axis: Δt (ms); y-axis: scale parameter α.

A contour plot dealing with the peak normalized LSC current for a phase-to-ground fault is presented in Fig. 10. This plot allows determining the temperature rise in the solid-state devices. A detailed thermal analysis for the system under study has been carried out in [13]. From this analysis, it resulted that, if the ambient temperature is less then or equal to 40 ° C, for LSC rms currents equal or less then 2 p.u., the junction limit temperature of 140 ° C is not reached. In contrast, for rms cur- rents above 2 p.u., the junction limit temperature is exceeded in few milliseconds. The authors' opinion is that this result can be extrapolated to other WECSs with similar operating condi- tions, but a dedicated study is necessary to determine the current limit of a generic WECS: if different IGBTs are used or the switching frequency is varied, the current limit is expected to be different.

The results displayed in Fig. 10 show that the rms current obtained for single-phase faults is always equal or less then 2 p.u. Single-phase faults will not result in exceeding of the solid-state devices thermal limits.

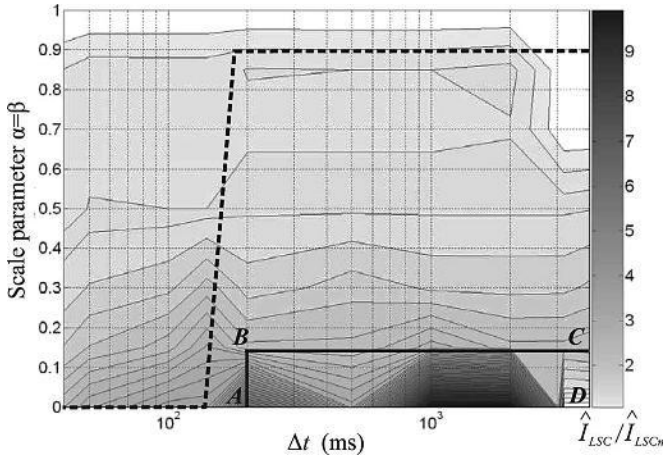

Fig. 11. Symmetrical sag: normalized LSC peak current contour plot. x-axis: Δt (ms); y-axis: scale parameter $\alpha = \beta$.

Fig. 11 displays a contour plot dealing with the peak normal- ized LSC current for symmetrical faults. Two trajectories are superimposed on the contour plot: the dotted line presents the LVRT curve shown in Fig. 7, and the rectangle ABCD defines the region where the currents through the solid-state devices ex- ceed 2 p.u.. System operation within the region ABCD cannot be guaranteed[2] ; however, since the dotted trajectory (i.e., LVRT re- quirements) and the rectangle do not intersect, the LVRT ability is not compromised.

From Fig. 11, one conclude that the highest LSC peak current amplitudes are obtained for residual voltage close to zero and relatively long fault durations. Since in case of severe faults, the protection devices will disconnect the WECS from the PCC, the earlier conditions are unlikely to be observed in real life. However, studying the system behavior for a wide spectrum of faults is necessary to ascertain the practical limitations of the system performance.

In Fig. 12, the contour plot illustrates the normalized LSC peak current for a line-to-line fault with $\beta = 0.7$ and $\alpha = 1$. The y-axis is the amplitude of the phase shift angle ε. This contour plot shows that the normalized LSC current amplitude is strongly dependent on phase angle ε, while the fault duration has a less significant influence. Since the limit of 2 p.u. is not reached, LVRT ability of the system is always verified for the fault conditions described in Fig. 12.

V. SYSTEM RESPONSE TO WIND SPEED VARIATIONS

A.Mechanical System Model

For steady-state analysis [8] and for system response to volt- age variations, mechanical dynamics have been ignored. This simplification has been made because [24].

1) During steady-state operation, wind speed is assumed constant; consequently, turbine rotating speed is constant and mechanical system dynamics does not affect WECS operation.
2) Since mechanical time constants are significantly larger than electrical time constants, the mechanical system oper- ation is not altered by the fast transients

caused by voltage dips.

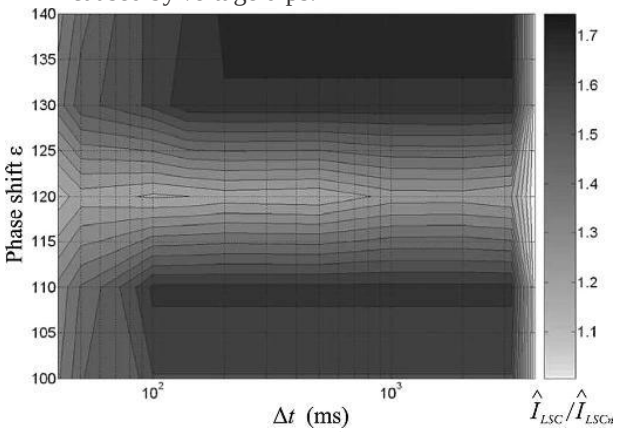

Fig. 12. Two-phase sag with phase shift: normalized LSC peak current contour plot. x-axis: Δt (ms); y-axis: phase shift ε ($\alpha = 1$ and $\beta = 1$).

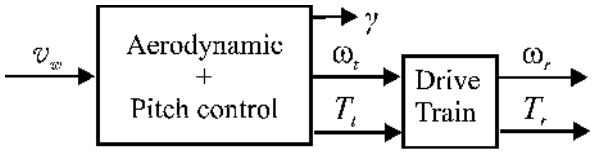

Fig. 13. Mechanical system model: input is the wind speed v_w, outputs are pitch angle γ, generator speed ω_r, and generator torque T_r

The mechanical system model consists of three major com- ponents, as depicted in Fig. 13:

1) **Aerodynamic model**: the relationship between wind speed v_u, turbine angular speed ω_t, and torque T_t is de- fined according to the tracking characteristic illustrated in Fig. 2.
2) **Drive train**: coupling between the wind turbine and the electric generator is represented by means of a two mass model [25]. The generator and the turbine are coupled by means of a torsional bar; damping is ignored.
3) **Pitch control model**: increase of the pitch angle γ allows power absorption reduction at wind speeds above the rated value. The pitch angle γ is a function of wind speed and rotor speed; a polynomial approximation is used to repre- sent this relationship [13], [26]. A rate limiter (10°/s) is included in the model to simulate blade maximum pitch speed.

The relationships between wind speed v_w, normalized shaft speed ω_r/ω_1, normalized power extracted from the turbine P_t/P_n, and pitch angle γ are listed in Table IV. The normalized power P_t/P_n and pitch angle γ are presented for both normal operation and derating (derating is applied for $v_w \geq 12$ m/s for the NLL assumed in the present study).

TABLE IV
RELATIONSHIPS BETWEEN WIND SPEED, TURBINE ANGULAR SPEED, POWER
EXTRACTED FROM THE WIND, AND
BLADE PITCH ANGLE

B. Simulation Results—Wind Speed Variation

Each simulation dealing with the system response to wind speed variation is carried out in two steps: first, the mechanical system response to wind speed variation is determined, and the torque and speed applied at the generator are obtained according to the model described in Fig. 13. Then, the solution of the electrical part of the system is obtained by using ω_r and T_r as input.

Case study A: Wind speed pattern is presented in Fig. 14(a). Three typical components [27] are included:

1) A major component with initial value equal to 14 m/s and
   a final value equal to 10 m/s. The transition takes place between $t = 5$ s and $t = 25$ s;
2) A low frequency ($f = 0.1$ Hz) component with amplitude equal to 0.1 m/s;
3) A random noise, with amplitude equal to 0.5 m/s and $f = 500$ Hz.

Pitch angle variation is illustrated in Fig. 14(b), where γ follows closely the major wind component (1) according to Table IV and reaches the value zero when the wind speed is less then or equal to 11 m/s (delays in the model are ignored since wind speed variation is relatively slow and the rate limiter is not activated). The low frequency fluctuation (2) are reproduced by γ only for wind speeds above 12 m/s, since γ control is activated only for speed above the rated value [26]. Finally, due to the blade's inertia, γ response is insensitive to the random noise (3).

The active power delivered to the grid is shown in Fig. 14(c) as the sum of stator and rotor active power. For $t \leq 5$, the active power is greater than unity as in Table IV; γ control helps maintaining a constant power absorption in this region. For $t > 5$ s, the active power amplitude reduces due to the decrease in wind speed. Two patterns are identified: for $5 \leq t \leq 17$ s, rotor active power only decreases, while stator active power is equal to 0.85 p.u.; for $17 \leq t \leq 25$ s, both stator and rotor power decrease and the slope of the active power curve is stiffer. For $t \geq 25$ s, the average power is $p/P_n \approx 0.5$, in agreement with the value listed in Table IV. In this region, active power follows the oscillations of wind speed, since γ control is not activated; these variations are minimal due to the low energy in the wind oscillations. Reactive power presented in Fig. 14(d) is constant since no reactive power control is activated. Grid current [see Fig. 14(e)] follows the pattern of active power; voltage at the PCC [see Fig. 14(f)] is constant due to the fact that a short line is assumed (= 1 km).

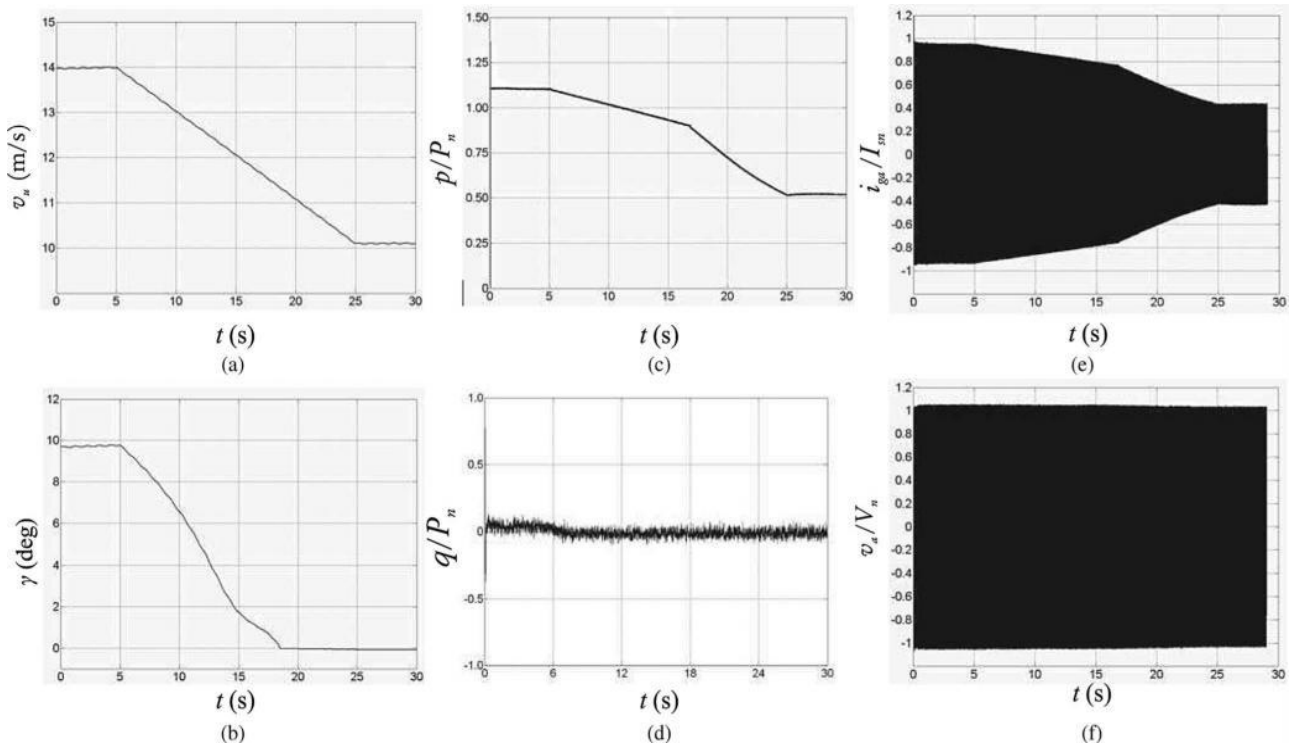

Fig. 14. Case study A, oscillograms: (a) wind speed, (b) pitch angle, (c) normalized active power, (d) normalized reactive power, (e) normalized grid current, and (f) normalized voltage measured at the PCC.

Case study B: The second case deals with wind speed increasing from 12 to 16 m/s for $2 \leq t \leq 3$, Fig. 15(a). Pitch angle control is activated when wind speed rises above 12 m/s: as shown in Fig. 15(b), γ is initially 1.7° and finally reached a new steady state value of 13.50 inagreement with Table IV. In this case, since the wind speed variation is relatively fast and severe, the variation of γ is determined by the rate limiter.

Wind speed variation causes oscillations of the shaft that couples the turbine to the electric generator. These oscillations appear also in the active power delivered to the grid, as shown in Fig. 15(c). Reactive power is constant since reactive power control is not activated, as shown in Fig. 15(d). The current oscillograms presented in Fig. 15(c) follows very closely the power oscillogram; the presence of low-frequency currents do not significantly affect the THD value.

Fig. 15(f) shows that voltage at the PCC reaches an unacceptable minimum amplitude equal to 0.8 p.u. This result is due to the fact that = 10 km is assumed for case study B, thus resulting in a large voltage drop on the feeder following grid current oscillation

VI. Reactive Power Control

From the oscillogram, as shown in Fig. 15(f), one learns that significant wind speed variations combined with a soft trans- mission line cause unacceptable voltage modulation at the PCC. Wind power plants based on DFIG technology have the ability to regulate reactive power flow by controlling the RSC and LSC operation [28]. This ability to regulate reactive power exchange with the grid can be used to implement reactive power control and the much needed controlling the RSC and LSC operation [28]. This ability to regulate reactive power exchange with the grid can be used to implement reactive power control and the much needed voltage regulation.

A block diagram that describes the concept of reactive power control and voltage regulation is presented in Fig. 16. In the stator voltage equivalent frame [29], the instantaneous imagi- nary power is expressed as [4]

$$q = v_d i_q \qquad (1)$$

where v_d is the normalized d-axis component of voltage mea- sured at the PCC and i_q is the normalized q-axis component of grid current.[3]

If the voltage at the PCC deviates from the rated value, an error signal $\Delta v_d = 1 - v_d$ is generated, as shown in the dashed lines of Fig. 16. The dotted lines deal with a second-error term.

In this study, the reference value of the q-axis current ($i_{q,\mathrm{ref}}$) is nil, given the unity power factor assumption. Due to wind speed variations and consequent current transients, the actual value of i_q differs from the reference value, and a second error term Δi_q is obtained.

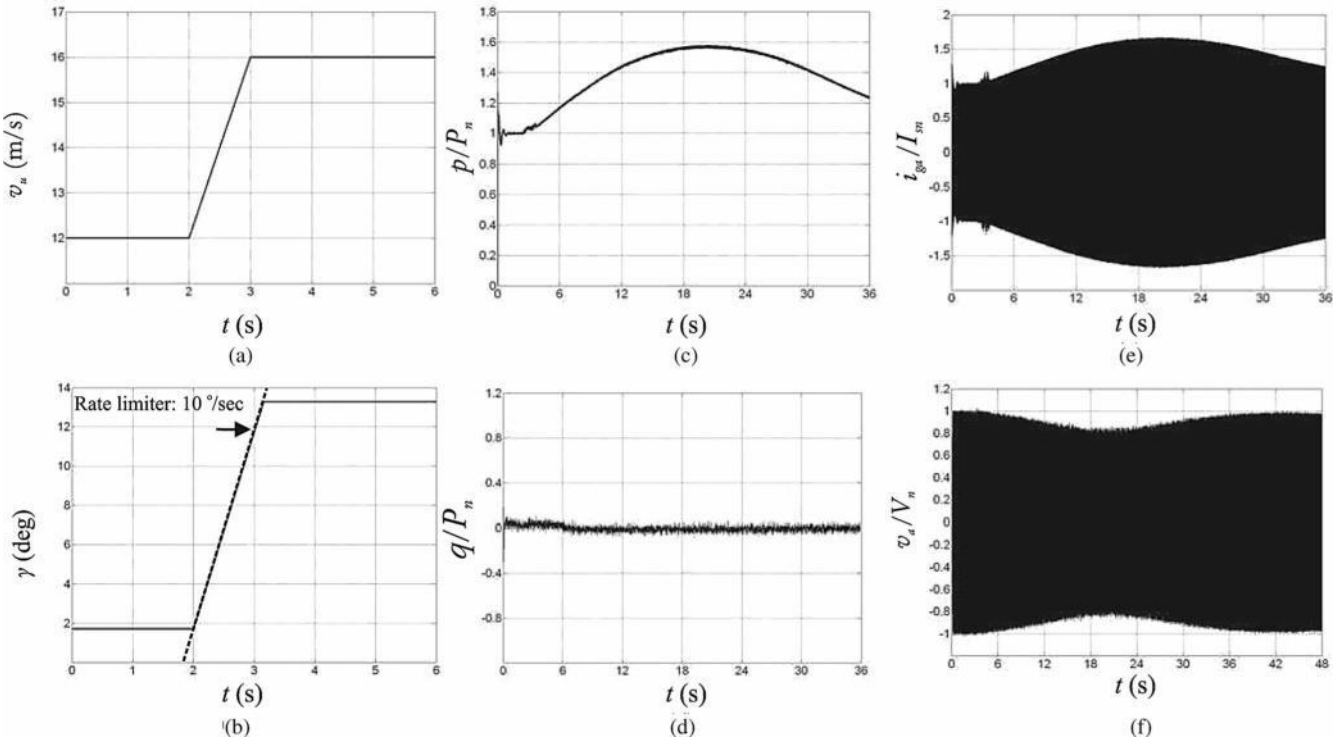

Fig. 15. Case study B, oscillograms: (a) wind speed, (b) pitch angle, (c) normalized active power, (d) normalized reactive power, (e) normalized grid current, and (f) normalized voltage measured at the PCC.

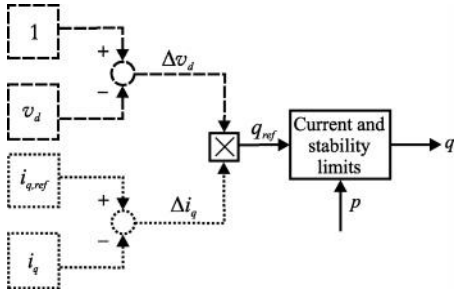

Fig. 16. Block diagram used for reactive power regulation: the reference signal q_{ref} is obtained from error terms Δv_d and Δi_q.

The product of Δv_d and Δi_q results in a reference instantaneous imaginary power q_{ref}; in steady-state operation, this term has value of zero. Reference imaginary power q_{ref} and instan- taneous active power p are the inputs to a block whose function is to define the maximum reactive power that can be provided by the WECS, based on generator stability and current limits. The output of this block is the instantaneous imaginary power q. The value q is used as one of the inputs to a block diagram intended to control the RSC operation [13].

Figs. 17 summarizes the results obtained for case study B when reactive power control is implemented. Reactive power variation takes place simultaneously with the current oscillation [see Fig. 17(b)], and as a result the grid voltage is almost constant [see Fig. 17(d)]. The active power and the grid current oscillograms are minimally affected by the voltage regulation, as one can observe by comparing the waveforms displayed in Fig. 17(a) and (b) with the ones displayed in Fig. 15(c) and (e).

VII. CONCLUSION AND DISCUSSION

The transient response of a WECS operating as power gener- ator and AF simultaneously has been presented. The conclusion of this study are as follows:

1) Harmonic compensation and transient response do not in-terfere. This is due to the fact that in the block diagrams for the control of the power converters, the fundamental current and voltage reference signals are separated from the harmonic signals. Voltage and wind speed variations contribute to determine the behavior of the fundamental components only; the harmonic currents flow results from the NLL characteristics. It has been observed that derating implemented when harmonic compensation is applied helps protecting the WECS during the transients.
2) LSC current is the quantity most severely affected by the transients following voltage variations. If derating is not applied, the use of a protection device is necessary to protect the solid-state devices [30], [31].
3) Reactive power regulation minimizes the voltage oscilla-tions at the PCC during wind speed transients: a reactive power regulator has been designed to perform this opera- tion.

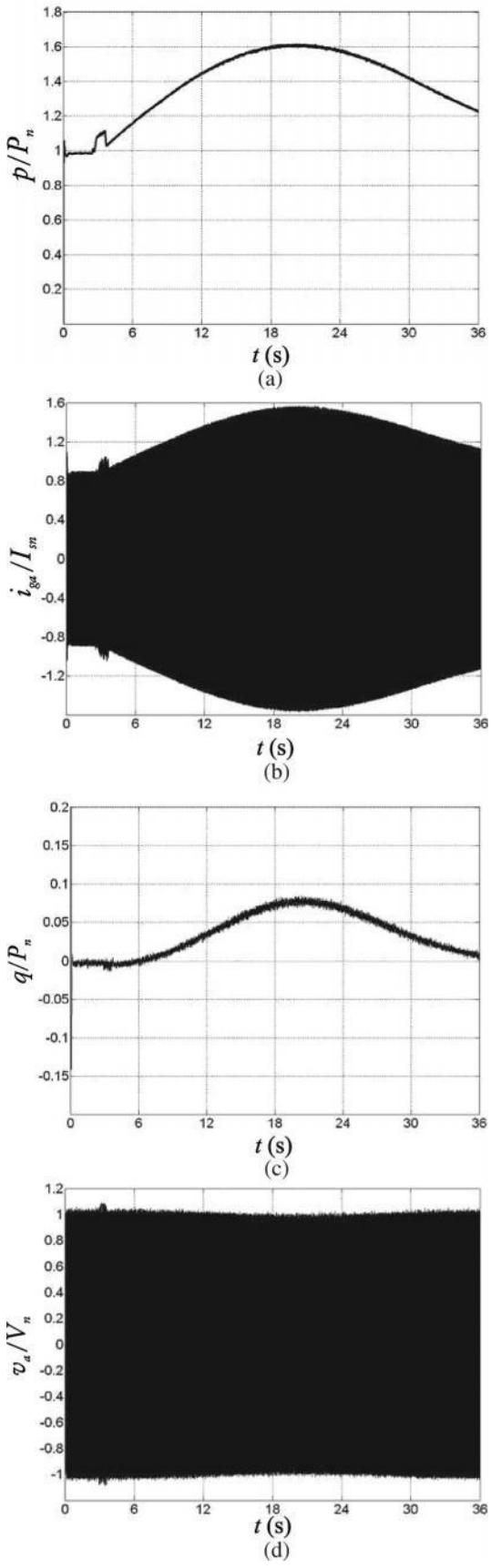

Fig. 17. Case study B, reactive power compensation is implemented: (a) nor- malized active power, (b) normalized reactive power, (c) normalized grid current, and (d) normalized voltage at the PCC.

The aforementioned conclusions apply to the specific WECS assumed in the present study and may be extended to systems with similar characteristics. Nevertheless, a number of design choices may affect the aforementioned conclusions; some of these choices have been discussed through the paper. For ex- ample, the effect of the length of the transmission line on the voltage profile after a wind speed variation has been addressed. Other factors contribute to determine the transient response of a WECS used as an AF, and they can be divided into three categories:

1) Electrical system: Phase jump during the fault has an im- portant role in determining the transient response and will require a dedicated analysis, while NLL characteristics and reactive power requirements affect steady-state oper- ation and derating.
2) Mechanical system: Blade and generator inertia affect the regulation of power absorption at high wind speed, thus impacting the quality of electric energy injected in the grid following severe wind speed variations.
3) Control system: To the authors' knowledge, no other pa- pers have been published regarding the transient response of WECS used as AF and power generator simultaneously. For this reason, a straightforward comparison with other methods cannot be carried out at the moment. Neverthe- less, further investigations on this topic may help identify- ing an optimized AF control that will allow: minimizing derating for the same harmonic current injection, meeting LVRT requirements, implementing reactive power regula- tion, improving current and voltage THDs.

From the aforementioned discussion, the results presented can be considered as a preliminary analysis dealing with the tran- sient response of a WECS used as AF. The results are promis- ing and motivate further research in this area to generalize the conclusions to a variety of WECS with different operating char- acteristics and to understand and identify the limitations of the proposed approach.

REFERENCES

[1] T. Ackermann, *Wind Power in Power Systems*. Hoboken, NJ: Wiley, 2005.
[2] L. H. Hansen, P. H. Madsen, F. Blaabjerg, H. C. Christersen, U. Lindhard, and K. Eskildsen, "Generators and power electronics technology for wind turbines," in *Proc. 27th Annu. Conf. IEEE Ind. Electron. Soc.*, Denver, CO, Nov. 29–Dec. 1, pp. 2000–2005.
[3] B. Singh, K. Al-Haddad, and A. Chandra, "A review of active filters for power quality improvement," *IEEE Trans. Ind. Electron.*, vol. 46, no. 5, pp. 960–971, Oct. 1999.
[4] H. Akagi, E. H. Watanabe, and M. Aredes, *Instantaneous Power Theory and Applications to Power Conditioning*. Hoboken, NJ: IEEE Press, 2007.
[5] M. T. Abolhassani, H. A. Toliyat, and P. Enjeti, "Stator flux oriented control of an integrated alternator/active filter for wind power applications," in *Proc. IEEE 2003 Int. Electr. Mach. Drives Conf.*, Madison, NJ, 1–4 Jun., pp. 461–467.
[6] M. T. Abolhassani, P. Niazi, H. A. Toliyat, and P. Enjeti, "Integrated doubly fed electric alternator/active filter (IDEA), a viable power quality solution, for wind energy conversion systems," *IEEE Trans. Energy Convers.*, vol. 23, no. 2, pp. 1642–650, Jun. 2008.
[7] E. Tremblay, A. Chandra, and P. Lagace, "Grid-side converter control of DFIG wind turbines to enhance power quality of distribution network," in *Proc. Power Eng. Soc. General Meeting*, Montreal, Canada, 18–22 Jun.2006, pp. 1542–1547.
[8] G. Todeschini and A. E. Emanuel, "Wind energy conversion system as an active filter: Design and comparison of three control systems,"

IET Renewable Power Generat., vol. 4, no. 4, pp. 341–353, Jul. 2010.

[9] G. Todeschini and A. E. Emanuel, "The DFIG as harmonic compensator by means of LSC modulation: Control system and derating for steady state performance," in *Proc. 25th IEEE Appl. Power Electron. Conf. Expo.*, Palm Beach, CA, Feb. 21–25, 2011, pp. 2096–2103.

[10] N. Mohan, T. M. Undeland, and W. P. Robbins, *Power Electronics: Con- verters, Applications and Design*, 3rd ed. Hoboken, NJ: Wiley, 2003.

[11] Powerex CM1000DU-34NF module, [Online]. Available: www.pwrx.com, 2009.

[12] B. K. Bose, *Power Electronics and AC Drives*, Upper Saddle River, NJ: Prentice-Hall, 2001.

[13] G. Todeschini, "Wind energy conversion systems as active filters: Steady- state transient analysis," in *Electrical Engineering—Circuit Design*, Saar- bruecken, Germany, VDM Publishing House, Jun. 2010.

[14] *Standard Test Procedure for Polyphase Induction Motors and Generators*, IEEE Power Engineering Society Standard 112, 1991.

[15] B. Andresen and K. Johansen, "Grid code and wind farm control requirements—What to control, why, where and how," in *Proc. 7th Int. Workshop Large Scale Integr. Wind Power Transmiss. Netw. Offshore Wind Farms*, Madrid, Spain, 26–27 May 2008, pp. 1–6.

[16] FERC Order No. 661A - Order on Rehearing and Clarification, *Intercon- nection for Wind Energy*, 2005.

[17] J. Morren and S. W. H. de Haan, "Ridethrough of wind turbines with doubly-fed induction generator during a voltage dip," *IEEE Trans. Energy Convers.*, vol. 20, no. 3, pp. 435–441, Jun. 2005.

[18] A. Mullane, G. Lightbody, and R. Yacamini, "Wind-turbine fault ride- through enhancement," *IEEE Trans. Power Syst.*, vol. 20, no. 4, pp. 1929–1937, Nov. 2005.

[19] S. Seman, N. Niiranen, S. Kanerva, and A. Arkkio, "Analysis of a 1.7 MVA doubly fed wind-power induction generator during power systems distur- bances," in *Proc. Nordic Workshop Power Ind. Electron.*, Trondheim, Norway, 14–16 Jun. 2004, pp. 1–6.

[20] W. Leonhard, *Control of Electrical Drives*. Electric driving. Berlin, Germany: Springer-Verlag, 2001.

[21] M. H. J. Bollen, *Understanding Power Quality Problems—Voltage Sags and Interruptions*. Piscataway, NJ: IEEE Press, 2000.

[22] J. Schlabbach, "Low voltage fault ride through criteria for grid connection of wind turbine generators," in *Proc. 5th Int. Conf. Eur. Electricity Market 2008*, Piscataway, NJ, 28–30 Mar., pp. 1–4.

[23] *The Technical Basis for the New WECC Voltage Ride-Though (VRT) Standard*, Wester Energy Coordinating Council, Jun. 13, 2007.

[24] A. D. Hansen and G. Michalke, "Fault ride-threou capability of DFIG wind turbines," *Sci. Direct—Renewable Energy*, vol. 32, no. 1, pp. 1594–1610, 2006.

[25] A. G. Abo-Khalil and L. Dong-Choon, "Dynamic modeling and control of wind turbines for grid-connected wind generation system," in *Proc. 37th IEEE Power Electron. Spec. Conf. 2006*, Jeju, Korea, 18–22 Jun., pp. 1–6. [26] S. Heier, *Grid Integration of Wind Energy Conversion Systems*.Hobo- ken, NJ: Wiley, 1998.

[27] J. S. Rohatgi and V. Nelson, *Wind Characteristics: An Analysis for the Generation of Wind Power*. Cayon, TX: Alternative Energy Institute, 1994.

[28] F. Blaabjerg and Z. Chen, *Power Electronics for Modern Wind Turbine*. (Synthesis Lectures on Power Electronics). San Rafael, CA: Morgan & Claypool, 2006.

[29] A. K. Jain, R. Tirumala, N. Mohan, T. Gjengedal, and R. M. Halet, "Har- monics and flicker control in wind farms," in *Wind Power Impacts Power Syst. Workshop*, Oslo, Norway, 17–18 Jun. 2002, pp. 1–5.

[30] J. Niiranen, "Voltage dip ride through of a double-fed generator equipped with an active crowbar," in *Proc. NordicWind Power Conf.*, Goteborg, Sweden, 1–2 Mar. 2004, pp. 1–4.

[31] J. Morren and S. W. H. de Haan, "Short-circuit current of wind turbines with doubly fed induction generator," *IEEE Trans. Energy Convers.*, vol. 22, no. 1, pp. 174–180, Mar. 2007.